THE NASCENT RED SEQUENCE AT $z \sim 2$ [1]

ANDREW W. ZIRM,[2] S. A. STANFORD,[3,4] M. POSTMAN,[5] R. A. OVERZIER,[2,6] J. P. BLAKESLEE,[7,8] P. ROSATI,[9]
J. KURK,[10] L. PENTERICCI,[11] B. VENEMANS,[12] G. K. MILEY,[13] H. J. A. RÖTTGERING,
M. FRANX, A. VAN DER WEL,[2] R. DEMARCO,[2] AND W. VAN BREUGEL[3,14]

ABSTRACT

We present new constraints on the evolution of the early-type galaxy color-magnitude relation (CMR) based on deep near-infrared imaging of a galaxy protocluster at $z = 2.16$ obtained using NICMOS on board the *Hubble Space Telescope*. This field contains a spectroscopically confirmed space overdensity of Lyα- and Hα-emitting galaxies that surrounds the powerful radio galaxy MRC 1138−262. Using these NICMOS data we identify a significant surface overdensity (=6.2 times) of red $J_{110} - H_{160}$ galaxies in the color-magnitude diagram (when compared with deep NICMOS imaging from the HDF-N and UDF). The optical-NIR colors of these prospective red-sequence galaxies indicate the presence of ongoing dust-obscured star formation or recently formed ($\lesssim 1.5$ Gyr) stellar populations in a majority of the red galaxies. We measure the slope and intrinsic scatter of the CMR for three different red galaxy samples selected by a wide color cut and using photometric redshifts both with and without restrictions on rest-frame optical morphology. In all three cases both the rest-frame $U - B$ slope and intrinsic color scatter are considerably higher than corresponding values for lower redshift galaxy clusters. These results suggest that while some relatively quiescent galaxies do exist in this protocluster both the majority of the galaxy population and hence the color-magnitude relation are still in the process of forming, as expected.

Subject headings: galaxies: clusters: individual (MRC 1138−262) — galaxies: evolution — galaxies: formation — galaxies: high-redshift — galaxies: stellar content

1. INTRODUCTION

The color-magnitude diagram is a powerful diagnostic of galaxy evolution and formation. The presence, as early as $z \sim 1.5$, of a prominent and low-scatter "red sequence" (RS) in galaxy clusters places useful constraints on the possible evolutionary pathways in galaxy color and luminosity (Mullis et al. 2005; Stanford et al. 2005, 2006; Bell et al. 2004; Faber et al. 2007). The red colors of the primarily early-type RS galaxies are due to the observed filters spanning the 4000 Å spectral break. The universality and prominence of the RS in appropriately chosen filters have been used to discover high-redshift clusters (e.g., Gladders & Yee 2005). Moreover, the defining characteristic of

galaxy clusters, i.e., the large numbers of galaxies all at the same redshift, allows the slope and intrinsic scatter of the RS to be measured with great precision. Based on studies of galaxy clusters at $z < 1.3$, the slope of the RS does not appear to evolve and therefore is more likely the by-product of the mass-metallicity relation as observed in local galaxy samples (e.g., Tremonti et al. 2004) rather than the result of a mass-age trend. The scatter, however, is likely due to the fractional age differences between the RS galaxies (e.g., Blakeslee et al. 2003). By constructing a set of model galaxies with different star formation histories and timescales it is possible to fit for the mean epoch of last significant star formation by matching the intrinsic scatter of the RS. Such studies at $z \sim 1$ have derived formation redshifts of $z_{form} \sim 2.0$–2.5 (e.g., Blakeslee et al. 2006; van Dokkum & van der Marel 2007). At redshifts beyond $z \sim 1.5$, however, the 4000 Å break moves into the near-infrared and galaxy clusters, and therefore the RSs have not been observed closer to the inferred epoch of formation for early-type galaxies. Hence, to uncover the younger or forming red sequence at higher redshifts requires deep near-infrared imaging of suspected (or, preferably, confirmed) protocluster fields.

We have undertaken a NICMOS imaging program to study the red galaxy population in a protocluster at $z = 2.16$. Broad and narrowband imaging, in both the optical and near-infrared, of the field surrounding the powerful radio galaxy MRC 1138−262 ($z = 2.16$) has identified more than 100 candidate companion galaxies. This target served as the proof of concept for the successful VLT Large Program summarized in Venemans et al. (2007). There are surface overdensities of line-emitting candidates (Lyα and Hα), X-ray point sources, submillimeter-selected galaxies, and red optical−near-infrared galaxies (Pentericci et al. 2002; Kurk 2003; Kurk et al. 2004a, 2004b; Croft et al. 2005; Stevens et al. 2003). Fifteen of the Lyα and nine of the Hα emitters have now been spectroscopically confirmed to lie at the same redshift as the radio galaxy. The $I - K$−selected extremely red objects (EROs; $I - K > 4.3$ Vega magnitudes) seem concentrated around the radio galaxy (RG) but have no spectroscopic redshifts at this

[2] Johns Hopkins University, 3400 North Charles Street, Baltimore, MD 21218; azirm@pha.jhu.edu.
[3] Institute of Geophysics and Planetary Physics, LLNL, L-413, Livermore, CA 94550.
[4] Physics Department, University California at Davis, 1 Shields Avenue, Davis, CA 95616.
[5] Space Telescope Science Institute, 3700 San Martin Drive, Baltimore, MD 21218.
[6] Max-Planck-Institut für Astrophysik, Karl-Schwarzschild-Strasse 1, 85741 Garching, Germany.
[7] Department of Physics and Astronomy, Washington State University, Pullman, WA 99164.
[8] Herzberg Institute of Astrophysics, NRC of Canada, 5071 West Saanich Road, Victoria, BC V9E 2E7, Canada.
[9] ESO-European Southern Observatory, Karl-Schwarzschild-Strasse 2, D-85748 Garching bei München, Germany.
[10] Max-Planck-Institut für Astronomie, D-69117 Heidelberg, Germany.
[11] Osservatorio Astronomico di Roma, I-00040 Monte Porzio Catone, Italy.
[12] IOA, Cambridge University, Madingley Road, Cambridge CB3 0HA, UK.
[13] Leiden Observatory, Leiden University, Postbus 9513, NL-2300 RA Leiden, The Netherlands.
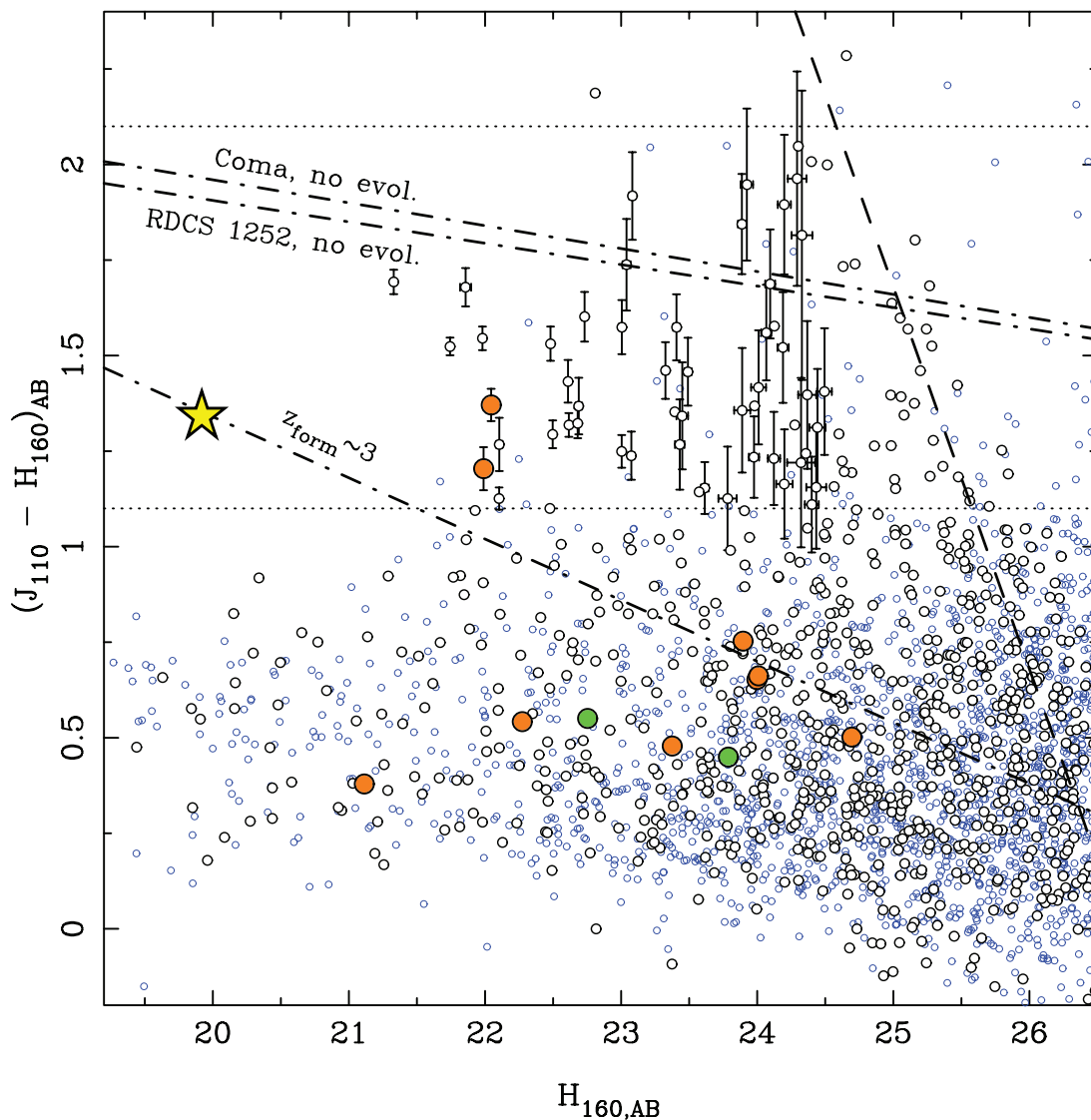[14] University of California, Merced, P.O. Box 2039, Merced, CA 95344.

FIG. 1.—$J_{110} - H_{160}$ vs. H_{160} color-magnitude diagram for the MRC 1138−262 NICMOS field (*open black circles*). The large yellow star represents the radio galaxy itself. The blue background points are from the NICMOS data of the Ultra Deep Field and Hubble Deep Field–North (Dickinson et al. 2000; Thompson et al. 2005). The deep fields cover 2.5 times the area of our observations. Also shown are the spectroscopically confirmed Hα (*orange filled circles*) and Lyα (*green filled circles*) emitters. The three dot-dashed lines show where the CMRs of lower redshift clusters would lie under different assumptions. The top line shows the Coma Cluster with no evolution, simply redshifted to $z = 2.16$ and observed through the NICMOS filters. The next line down is the same but for the $z = 1.24$ cluster RDCS 1252. Finally, if we passively de-evolve RDCS 1252 to redshift $z = 2.16$ (almost exactly 2 Gyr), assuming a median age for the 1252 galaxies of about 3 Gyr (or $z_{form} \sim 3$), we get the third line.

time. However, by obtaining deep images through the NICMOS J_{110} and H_{160} filters, which effectively span the 4000 Å break at $z = 2.16$, accurate and precise colors and basic morphological parameters can be measured for the red galaxy population. In this paper we present the first results from this project. The article is organized as follows: in § 2 we describe the data and their reductions, in § 5 we present the comparison between the red galaxy counts in this field and in deep field data, and in § 6 we present the full color-magnitude diagram and our fits to the "red sequence." We use a $(\Omega_\Lambda, \Omega_M) = (0.73, 0.27)$, $H_0 = 71$ km s^{-1} Mpc^{-1} cosmology throughout. At $z = 2.16$ 1″ is equivalent to 8.4 kpc. All magnitudes are referenced to the AB system (Oke 1974) unless otherwise noted.

2. OBSERVATIONS, DATA REDUCTIONS, AND PHOTOMETRY

The NICMOS instrument on board *HST* is capable of deep near-infrared imaging more quickly than from the ground but with a relatively small field of view ($51'' \times 51''$). In the case of MRC 1138−262 we know that galaxies are overdense on the scale of a few arcminutes (Kurk et al. 2004b; Croft et al. 2005) and are thus well suited for observations with NICMOS camera 3 on *HST*. We used 30 orbits of *HST* time to image 10 of the 24 confirmed members and ∼70 of the candidate (narrowband excess sources and EROs) protocluster members in both the J_{110} and H_{160} filters. We used seven pointings of NICMOS camera 3 in both filters and one additional pointing in H_{160} alone. This single "outrigger" H_{160} pointing was included to obtain rest-frame optical morphological information for a small concentration of candidate members. These observations reach an AB limiting magnitude ($m_{10\,\sigma}$; 10 σ, 0.5″ diameter circular aperture) of $m_{10\,\sigma} = 24.9$ mag in J_{110} and $m_{10\,\sigma} = 25.1$ mag in H_{160}. The same field was imaged in the g_{475} ($m_{10\,\sigma} = 27.5$ mag) and I_{814} ($m_{10\,\sigma} = 26.8$ mag) filters using the wide-field channel of the Advanced Camera for Surveys on *HST* as part of a guaranteed time program (No. 10327; Miley et al. 2006). These optical data are useful for
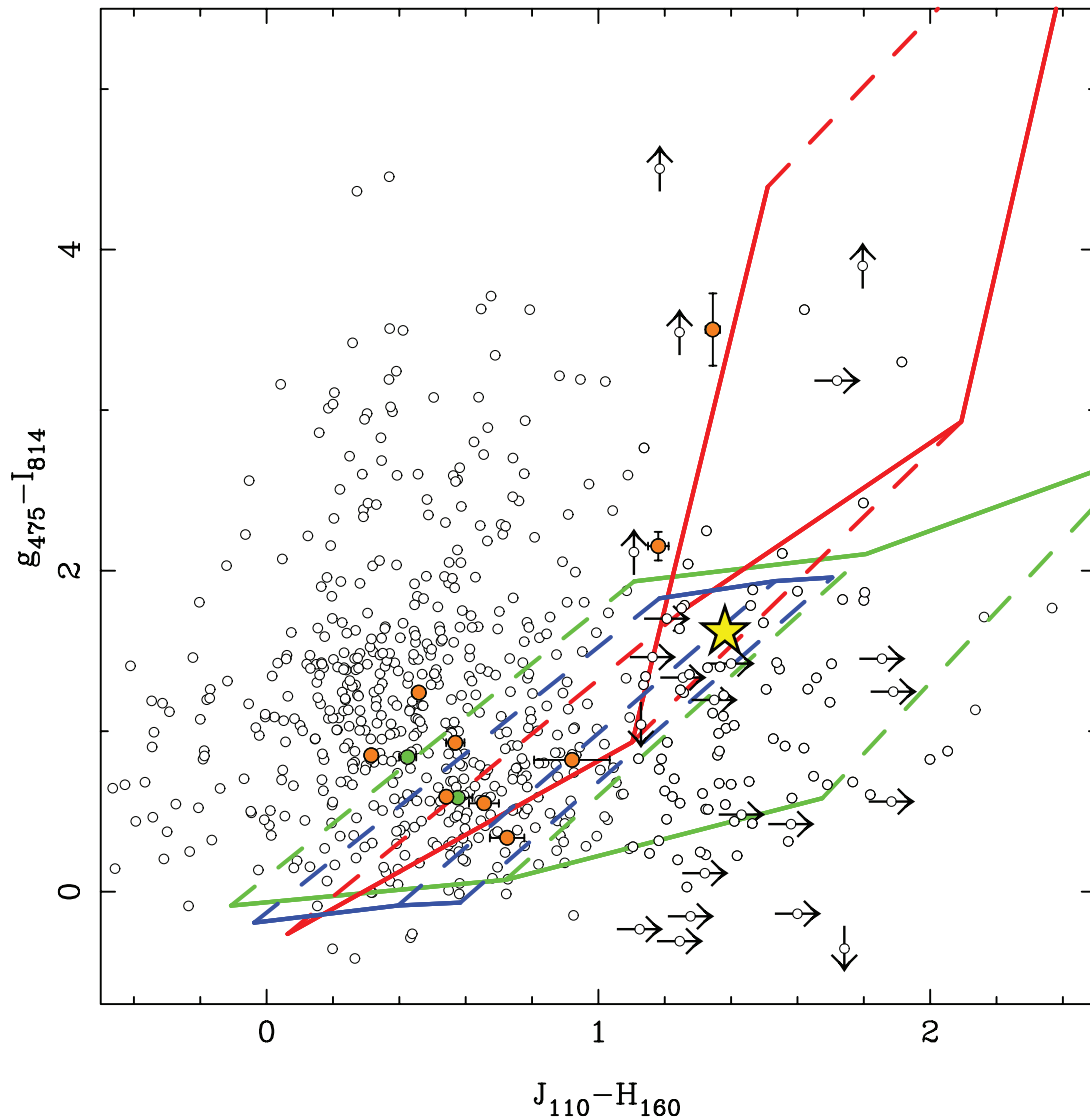
Fig. 2.—A $g_{475} - I_{814}$ vs. $J_{110} - H_{160}$ color-color diagram using the ACS and NICMOS data. Arrows represent limits where the galaxy is only detected in a single band for that color. Filled circles indicate spectroscopically confirmed Lyα- (*green*) and Hα- (*orange*) emitting protocluster members. The yellow star indicates the radio galaxy. The blue, green, and red grids indicate the regions occupied by galaxies with an exponentially decaying star formation rate $\tau = 0.15$ Gyr (*red*), $\tau = 0.4$ Gyr (*green*), and $\tau = 1000$ Gyr (*blue*) at $z = 2.16$ for three ages (0.1, 1, and 3 Gyr; connected by solid lines) and two different extinctions [$E(B - V) = 0.0, 1.0$] (connected by dashed lines).

their higher angular resolution and their coverage of the rest-frame far-UV, thus extending the observed SEDs of candidate protocluster members to shorter wavelengths where young stars and ongoing star formation dominate the emitted spectrum. In particular, the g_{475} and I_{814} data allow us to partially differentiate obscured star formation from evolved stellar populations in the candidate RS galaxies.

The NICMOS images were reduced using the on-the-fly reductions from the *HST* archive, the IRAF task `pedsky`, and the dither/drizzle package to combine the images in a mosaic. The dither offsets were calculated using image cross-correlation and were refined with one further iteration of cross-correlation. Alignment of the pointings relative to each other was accomplished using a rebinned version of the ACS I_{814} image as a reference. The final mosaic has a pixel scale of $0.1''$. Galaxies were selected using the H_{160}-band image for detection within SExtractor (Bertin & Arnouts 1996). We used a 2.2 σ detection threshold with a minimum connected area of 10 pixels. We also corrected the NICMOS data for the count-rate-dependent nonlinearity (de Jong

2006). Total galaxy magnitudes were estimated by using the MAG_AUTO values from SExtractor.

The $J_{110} - H_{160}$ colors were determined by running SExtractor (Bertin & Arnouts 1996) in two-image mode using the H_{160} image for object detection and isophotal apertures. The J_{110} image was point-spread function (PSF) matched to the H_{160} band. The resulting colors and magnitudes are shown in Figure 1. For galaxies that are not detected at 2 σ significance in the J_{110} band (those to the right of the thick dashed line, representing $J_{110, tot} > 26.7$, in Fig. 1) we consider the color to be a lower limit.

We also measured similarly PSF-matched, isophotal colors using the two ACS bands and have used them to construct a $g_{475} - I_{814}$ versus $J_{110} - H_{160}$ color-color diagram (Fig. 2). We compared these colors to those of model SEDs for different ages, star formation histories, and dust extinctions. Using the 2007 Charlot & Bruzual population synthesis models we have constructed spectral energy distributions for galaxies with an exponentially decaying star formation rate with time constants of $\tau = 0.15$, 0.4, and 1000.0 Gyr (the red, green, and blue grids in

Fig. 2, respectively). Each model's colors are calculated for ages of 0.1, 1, and 3 Gyr and for $E(B-V) = 0.0$ and 1.0. Aging of the population moves primarily the $J_{110} - H_{160}$ color to the red, while the dust extinction significantly reddens the $g_{475} - I_{814}$ color. From this analysis it appears that the $\tau = 0.4$ Gyr model represents well the colors of a majority of the red $J_{110} - H_{160}$ galaxies.

To extend the wavelength coverage for the protocluster galaxies we also incorporated ground-based U_n-band data from LRIS-B on the Keck telescope, K_s-band imaging from VLT/ISAAC, and three-band IRAC imaging (the 3.6, 4.5, and 5.8 μm bands) from the *Spitzer Space Telescope*. The Keck U-band data (PI W. van Breugel) were obtained in late January and early February of 2003. The ISAAC data (PI G. Miley) were taken in period 73 in service mode. The *Spitzer* data are from the IRAC guaranteed time program (PI G. Fazio, program No. 17). We have smoothed the imaging data for all bands, apart from the IRAC data, to match the resolution of the U_n-band image (approximated by a FWHM $\sim 1''$ Gaussian). We then used SExtractor to measure galaxy magnitudes within a $0.5''$ radius circular aperture for each smoothed image. To incorporate the IRAC data, which has much poorer angular resolution, we derived aperture magnitudes that were then corrected to match the smoothed data. These aperture corrections were derived using the photometric curves of growth for 20 stars in the field. The resulting catalog was used to generate photometric redshift estimates as described below in § 3.

3. PHOTOMETRIC REDSHIFTS

We have used the ACS (g_{475}, I_{814}), NICMOS (J_{110}, H_{160}), ground-based U_n band from Keck/LRIS-B, K_s-band imaging from VLT/ISAAC and *Spitzer*/IRAC imaging to estimate photometric redshifts for our H_{160}-band–selected sample. We input a catalog of aperture galaxy magnitudes, based on the matched, smoothed images described above, into the Bayesian photometric redshift code (BPZ) of Benítez (2000) using a uniform prior. We felt that the default prior, based on optical galaxy selection and spectroscopy in the HDF-N, would not necessarily represent the redshift distribution for our near-infrared–selected galaxies. We generated our own extensive set of template spectral energy distributions using the models of Charlot & Bruzual (2003, 2008, in preparation). All these SEDs are τ models with values for $\tau = [0.15, 0.4, 1.0, 2.0, 1000.0]$ Gyr and ages = $[0.05, 0.1, 0.5, 1.0, 2.0, 3.0]$ Gyr. We also included models with internal dust extinction ranging from $E(B-V) = [0.0, 0.1, 0.3, 0.5, 0.75, 1.0]$ mag and metallicity of $(Z/Z_\odot) = [0.3, 1.0, 2.5]$.

We focused particular attention on the $J_{110} - H_{160}$–selected surface overdensity. In the top panel of Figure 3 we present the high-confidence (>95%) photo-z distribution for the NIR color–selected $[1.1 \leq (J_{110} - H_{160}) \leq 2.1]$ subsample. We ran extensive simulations by redshifting our template set, adding appropriate photometric errors and using BPZ to recover the redshifts. The yellow curve represents the redshift selection function for this color cut, template set, and filters, assuming that these model galaxies follow a uniform $N(z)$ over this redshift interval. The simulation results were free of significant systematic errors, and the random errors are estimated to be $\delta z/z \sim 0.1$. Based on these SED fits, the approximate luminosity-weighted ages of the red galaxies lie between 1 and 2.5 Gyr and their stellar masses are of the order of a few times $10^{10} M_\odot$. These stellar masses are reasonable as are the absolute magnitudes (see Fig. 6). More detailed SED modeling is deferred to a future paper.

There is a clear excess of galaxies between $z = 2.0$ and 2.5. For each galaxy fit by BPZ we have generated the full redshift
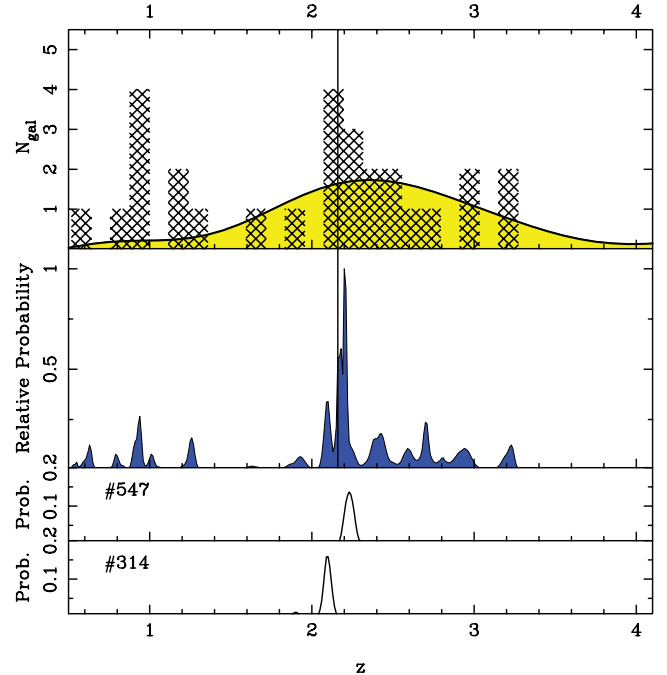

Fig. 3.— *Top*: Distribution of high-confidence (>95%) photometric redshifts and their selection function assuming a uniform $N(z)$ for our model template galaxies (*yellow curve*) for $1.1 \leq (J_{110} - H_{160}) \leq 2.1$ galaxies in the MRC 1138−262 NICMOS field. The peak between $z = 2.1$ and 2.4 is statistically highly significant. *Middle*: Sum of redshift probability distributions for all the galaxies in the top panel; 38.5% of the total probability is contained in the redshift interval from 2 to 2.3. *Bottom two panels*: Two examples of the probability distribution function for individual galaxies.

probability distribution. In the middle panel of Figure 3 we show the H_{160}-band weighted average of these probability distributions. There is a clear peak (containing 38.5% of the total probability compared to only 17% of the total selection function in the same redshift interval) between $z = 2.0$ and 2.3, consistent with the significant peak in the redshift histogram itself.

4. NICMOS GALAXY MORPHOLOGIES

NICMOS camera 3 provides good angular resolution over its entire field of view. The FWHM of the PSF in our final mosaic is $\approx 0.27''$. To exploit this resolution we have used the GALFIT code (Peng et al. 2002) to fit analytic Sérsic surface-brightness profiles (Sérsic 1968) to all the $H_{160} \leq 24.5$ sources in our H_{160}-band mosaic. A model point-spread function was created for each of these galaxies individually by generating a TinyTim simulated PSF (Krist 1993) at the galaxies' positions in each exposure and then drizzling these PSFs together in exactly the same fashion as for the data themselves (see Zirm et al. 2007). We restricted the Sérsic index, n, to be between 1 and 5. We will present a full analysis of the morphologies of these galaxies in a future paper. For the current work we use these derived sizes and profile shapes to assist us in selecting the morphological "early-type" members of the red galaxy population.

In Figure 4 we show the distribution of galaxy ages derived via these SED fits as parameterized by the τ value for the best-fitting model for those galaxies with high and low Sérsic index ($n \geq 2.5$, *red line*, and $n < 2.5$, *blue line*). It is clear that while there is substantial overlap between these distributions they are not identical and that they differ in the sense that one might expect, namely, that the concentrated galaxies appear to be comprised
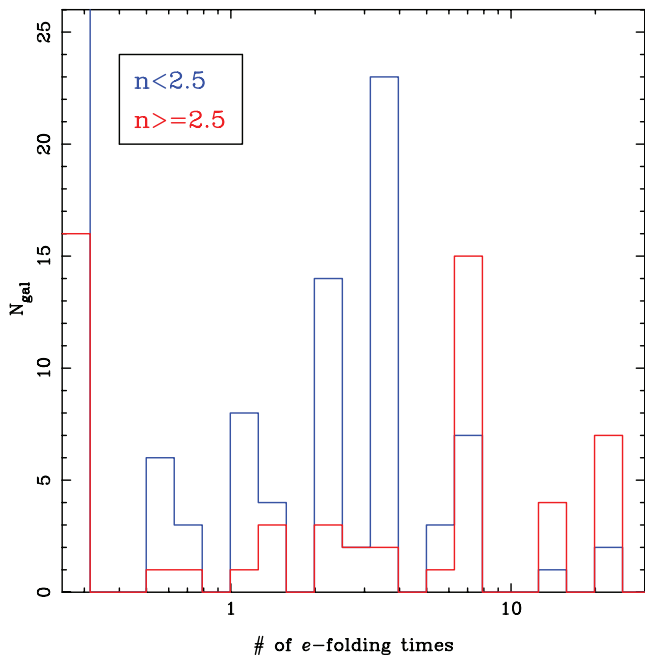
Fig. 4.—Distribution of inferred stellar ages (in terms of τ) for both the concentrated ($n \geq 2.5$; *red line*) and diffuse ($n < 2.5$; *blue line*) galaxies, which are well resolved in the NICMOS data. Constant star formation models, for which the *e*-folding time is infinite, are placed at the left-hand edge of the plot. The blue and red distributions are quite different. Of particular note is that the most evolved galaxies generally have high *n*, while the low-*n* galaxies dominate the star-forming population.
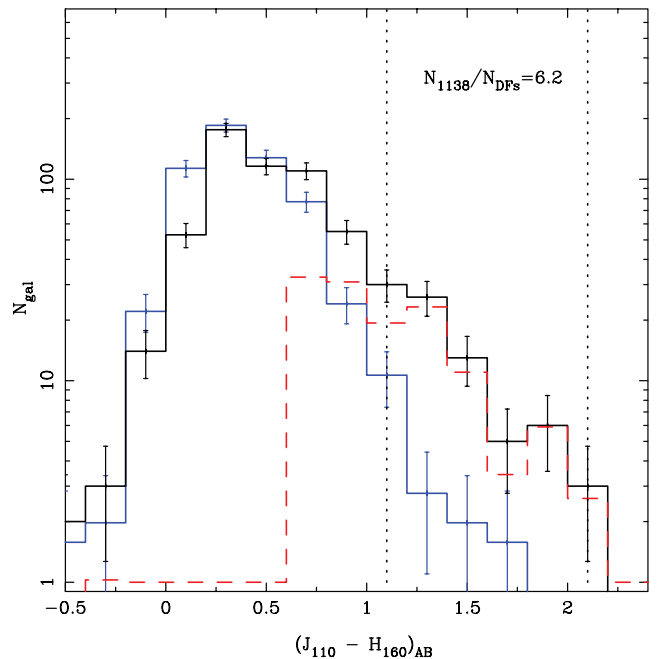

Fig. 5.—Histogram of the color distributions for the 1138 and deep fields (*blue*). The deep field data have been normalized by total area to the 1138 data. Note the clear excess of red galaxies in the 1138 field. At $1.1 \leq (J_{110} - H_{160}) \leq 2.1$ (*vertical dotted lines*) for galaxies brighter than the $2\,\sigma$ J_{110}-band limit (*dashed line*) there is an overdensity of a factor of 6.2 in the 1138 field.

of older stellar populations. This trend gives us some confidence in trying to select the "early-type" galaxies using these data, which is important for our discussion of the color-magnitude relation in § 6.

5. SURFACE OVERDENSITY OF RED GALAXIES

To compare this protocluster field to more generic "blank" field data we have compiled catalogs for the public NICMOS data in both the Hubble Deep Field–North (HDF–N) and the Ultra Deep Field (UDF; Dickinson et al. 2000; Thompson et al. 2005). Figure 1 shows the $J_{110} - H_{160}$ color-magnitude diagram (*open black circles*) and the color distributions for both the MRC 1138−262 and the combined HDF–N and UDF galaxy catalogs (*blue circles*). The deep field data were also H_{160}-band selected. The area of the two deep fields is roughly 2.5 times the area of our protocluster observations. We have applied no correction to the deep field number counts to account for clustering in those fields. The color histogram in Figure 5 shows the area-normalized galaxy counts from the two deep fields (*blue line*) and from the 1138 field to the same ($2\,\sigma$) limiting magnitude of $J_{110} = 26.7$ mag (AB). The red dashed line shows the difference between the two color distributions. It is clear that the radio galaxy field is overdense in red galaxies by a large factor. For sources with colors in the range $1.1 \leq (J_{110} - H_{160}) \leq 2.1$, the horizontal (vertical) dotted lines in Figure 1 (Figure 5), and brighter than our J_{110}-band $2\,\sigma$ limit (26.7), we calculate an area-normalized overdensity of 6.2 when compared to the deep field data. We note that the exact value of the measured overdensity is rather sensitive to systematic color offsets between the protocluster and deep field data. A redward shift of 0.05 for the deep field galaxies would lower the measured overdensity to 5.0. However, we are confident that these systematic offsets remain small (<0.05 mag)

since we have used the same instrument, filters, selection technique and photometric code with very similar input parameters for both the deep field and 1138 data sets. Looking back at Figure 2 we can see that many of the spectroscopically confirmed line emitters (*filled blue circles*) and red galaxies in the overdensity are well represented by the $\tau = 0.4$ Gyr model (*green lines*) at different ages and extinctions.

This current work is not the first to observe red galaxies in this field. Kurk et al. (2004b) identified a small (∼1.5 times) surface overdensity of extremely red objects (EROs; $I - K > 4.3$ Vega magnitudes) using ground-based I- and K-band data. Many of these EROs are also identified as red in the NICMOS $J_{110} - H_{160}$ color. More recently Kodama et al. (2007) observed this field using the wide-field NIR imager, MOIRCS, on the Subaru telescope. These authors found several bright (presumably massive) red galaxies over a wider field of view but to shallower depths than the NICMOS data presented here. Twenty-four of their color-selected protocluster candidates are within our NICMOS mosaic. Twenty-three of the 24 are identified in our data as being red in $J_{110} - H_{160}$. Furthermore, 18 of the 94 galaxies that satisfy our color criteria (and have $J_{110} < 26.67$) are also identified by Kodama et al. as protocluster candidates. The much larger number of red galaxies in the NICMOS data is primarily due to fainter galaxies detected at high significance in our deeper data.

6. AN EMERGENT RED SEQUENCE?

To study the colors and magnitudes of these galaxies in more detail and to possibly identify a red sequence in the 1138 field we have split the galaxies into three subsamples defined by $J_{110} - H_{160}$ color, photometric redshift and morphology (Sérsic index). The first sample (sample A) comprises all 56 galaxies with $1.1 \leq (J_{110} - H_{160}) \leq 2.1$ and $H_{160} < 24.5$ and includes the radio galaxy itself. Sample B is made up of all 28 galaxies with a robust photometric redshift between 2.0 and 2.5 and $J_{110} - H_{160} > 0.75$

TABLE 1
PROPERTIES OF RED GALAXIES IN THE MRC 1138−262 FIELD: $H_{160} < 24.5 \wedge 1.1 \leq (J_{110} - H_{160}) \leq 2.1$

ID	z_{phot}[a]	Odds[b] (BPZ)	SED Type[c]	Sérsic Index (n)	r_e (arcsec)	r_e (kpc)	H_{160}[d] (AB mag)	$U_n - g_{475}$ (AB mag)	$g_{475} - I_{814}$ (AB mag)	$I_{814} - J_{110}$ (AB mag)	$J_{110} - H_{160}$ (AB mag)
507...........	2.09	1.00	1.00	5.0 ± 0.4	0.24 ± 0.01	1.99 ± 0.08	22.50 ± 0.01	...	...	2.22	1.52
314...........	2.10	1.00	1.00	5.0 ± 0.7	0.15 ± 0.01	1.28 ± 0.05	23.03 ± 0.01	1.92	1.38	1.89	1.29
586...........	2.10	1.00	1.00	5.0 ± 0.3	0.40 ± 0.03	3.34 ± 0.23	21.77 ± 0.01	1.80	1.89	2.22	1.61
547...........	2.23	1.00	1.00	5.0 ± 0.6	0.12 ± 0.00	1.02 ± 0.04	22.70 ± 0.01	1.30	1.13	1.67	1.36
493...........	2.25	1.00	1.00	3.5 ± 0.3	0.56 ± 0.04	4.72 ± 0.36	22.75 ± 0.02	0.63	1.28	2.19	1.64
312...........	2.42	1.00	1.00	5.0 ± 0.3	0.38 ± 0.02	3.20 ± 0.19	22.00 ± 0.01	...	1.45	1.94	1.55
127...........	2.44	1.00	1.00	2.7 ± 0.6	0.12 ± 0.02	1.01 ± 0.18	22.64 ± 0.01	0.34	1.04	1.37	1.40

[a] The errors on these photometric redshifts are approximately 0.1–0.2.
[b] The ODDS parameter approaches unity when the probability distribution function has a single narrow peak.
[c] Best-fit broadband template type: 0: dusty and star forming, 1: quiescent.
[d] Total magnitudes based on the SExtractor MAG_AUTO parameter.

and $H_{160} < 26.0$. This liberal color cut is included to select galaxies that comprise the large observed surface overdensity. Finally, sample C contains seven galaxies with the same photometric redshift cut but that also have well-resolved H_{160}-band surface-brightness profiles with Sérsic index $n > 2.5$. All of these galaxies' SEDs are also best fit by models with relatively little ongoing star formation. We use a limit of age $\geq 4\tau$ (cf. Grazian et al. 2007). Therefore, sample C mimics the color, morphological, and photometric redshift selection of early-type galaxies in clusters at $z \lesssim 1$. The photometry, photo-zs, and sizes of the sample C galaxies are listed in Table 1, their rest-frame color-magnitude distributions are shown in Figure 6 and the two-dimensional spatial distribution of the sample A galaxies is plotted in Figure 7. We note that because the measured overdensity is a factor of 6, we statistically expect one of every seven sample A galaxies to be a field galaxy. However, this should not effect our results significantly.

For these three sample selections we have fit a line and measured the intrinsic scatter about that best-fit line (see Fig. 6). For comparison to lower redshift galaxy clusters we have transformed our observed $J_{110} - H_{160}$ color and H_{160} magnitudes into rest-frame $U - B$ and B (Vega), respectively, using the following expressions:

$$(U - B)_{rest} = 0.539(J_{110} - H_{160})_{obs} - 0.653, \quad (1)$$

$$M_{B,rest} = H_{160,obs} - 0.170(J_{110} - H_{160})_{obs} - 43.625. \quad (2)$$

The small color corrections used in these relations were derived using a family of τ-models with a range of ages (0.1–12 Gyr), τ (0.1–5 Gyr), and three metallicities (0.4, 1, and 2.5 $Z_{\odot}$).

To fit the "CMR" we used a bootstrap resampling technique to estimate the error on the fitted slope. Then, by assuming that all the red galaxies lie on this fit line, we ran Monte Carlo realizations of the contribution of the photometric errors to the observed color scatter about the fit line; i.e., by fixing a color-magnitude relation we calculate the measurement scatter with zero intrinsic scatter. We then calculate the intrinsic scatter by subtracting (in quadrature) the estimated measurement scatter from the observed scatter. We show these fits (*solid line*) and the intrinsic scatters (*dotted lines*) for the three samples (A, B, and
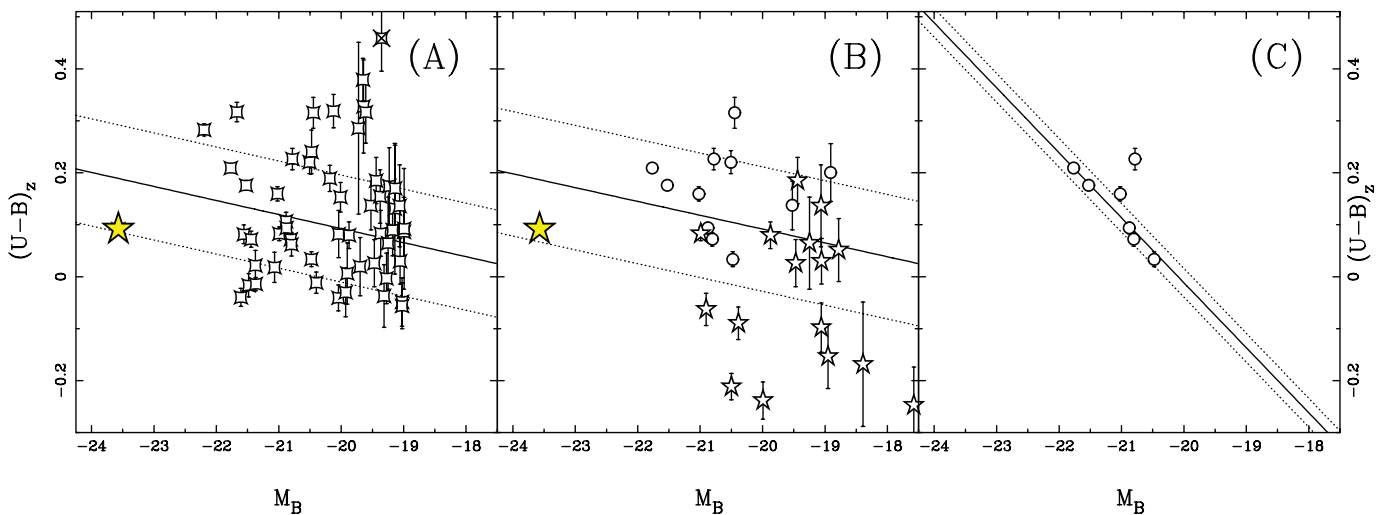

FIG. 6.—Linear fits to the rest-frame $U - B$ (Vega) color-magnitude diagrams for three different subsamples of the H_{160}-band–selected NICMOS sample. Panel A shows the fit (*solid line*) and intrinsic scatter (1 σ; *dotted lines*) for a sample selected to have $1.1 \leq (J_{110} - H_{160}) \leq 2.1$. The crossed out points are those which are rejected as outliers in more than half of the realizations (see § 6). Both the observed and intrinsic scatter are smaller than the initial color cut. Panel B shows the fit and intrinsic scatter for a photometric redshift–selected sample with $2.0 < z_{phot} < 2.5$. The stars indicate galaxies whose preferred photometric template has an age $<4\tau$, while circles represent galaxies older than this limit. Panel C shows the fit and scatter for those galaxies which meet the same redshift cut but also are well resolved with a high Sérsic index ($n > 2.5$) and best fit by an age $\geq 4\tau$ template.
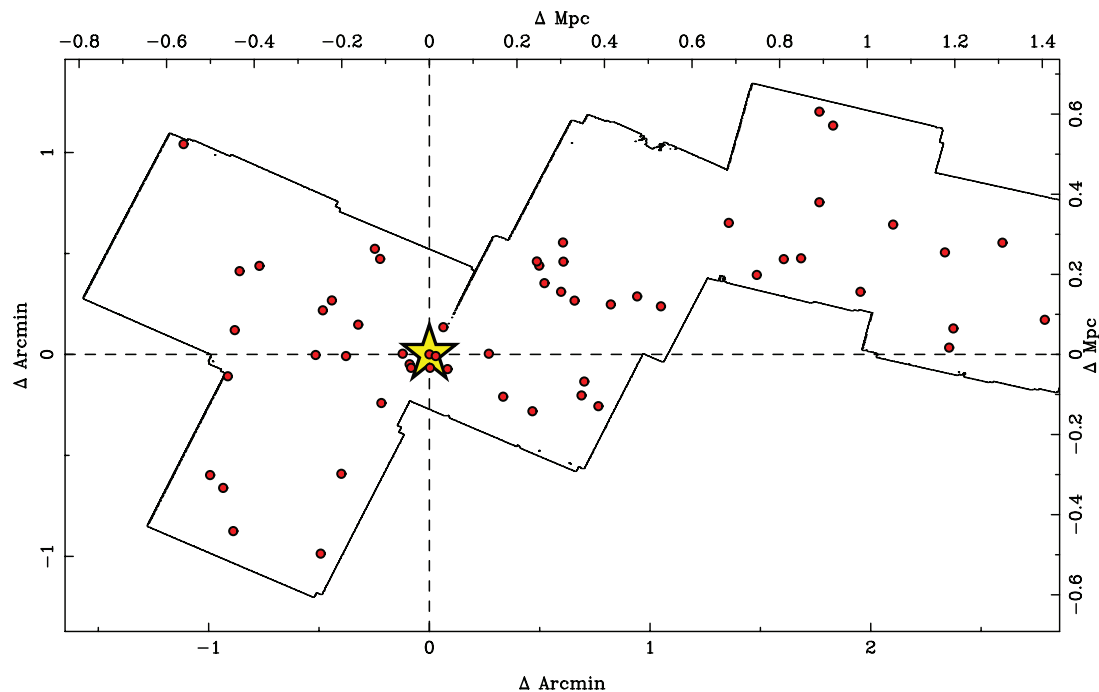
FIG. 7.—Spatial distribution of galaxies (*red circles*) relative to the radio galaxy MRC 1138−262 (*yellow star*) for the color-selected sample defined in the text (A) and shown in the first panel of Fig. 6. The irregular black outline encloses the coverage of the seven NICMOS camera 3 pointings with both J_{110} and H_{160} imaging.

C) in Figure 6. The fits to both samples A and B have nearly identical rest-frame $U − B$ slopes, 0.027 and 0.026, respectively, and intrinsic scatters (0.10 and 0.12). While these slopes are comparable to those found for the well-populated lower redshift cluster CMRs, the intrinsic scatters are considerably higher. However, the scatter measured for the eight galaxy sample C is comparable to that of the lower redshift samples but with a much steeper slope (0.130). When these scatters are compared to model predictions based on lower redshift clusters (specifically RDCS 1252.9−2927 at $z = 1.24$; Gobat et al. 2008) we find that the 1138 protocluster has lower than predicted scatter. This may suggest that the 1138 protocluster is in a more advanced evolutionary state than RDCS 1252 was at $z = 2.2$.

We have calculated three representative color-magnitude relations for comparison to the colors and magnitudes of the red galaxies (three dot-dashed lines in Fig. 1). We have taken two lower redshift clusters, Coma at $z = 0.023$ and RDCS 1252.9−2927 at $z = 1.24$, and transformed them to the observed filters and $z = 2.16$ under the assumption that the colors do not evolve. In this no-evolution case (two dot-dashed lines in Fig. 1) the CMRs appear at the red edge of the observed overdensity. There is almost exactly 2 Gyr of cosmic time between $z = 2.16$ and 1.24 in our adopted cosmology. From Blakeslee et al. (2003) we know that the median redshift of last significant star formation for the RDCS 1252 galaxies is between $z = 2.7$ and 3.6. Therefore, if we observe those galaxies at $z = 2.16$ they will be significantly younger and hence bluer. In fact, this passively de-evolved line (bluest dot-dashed line in Fig. 1, labeled "$z_{form} \sim 3$") does fall blueward of the red galaxy overdensity. We discuss the implications for these comparisons in § 7.

We have also translated the Kodama et al. (2007) ground-based $J − K$ colors to our NICMOS filters assuming that all the red galaxies lie at $z = 2.16$. These bright galaxies also fall along the passively de-evolved line with the radio galaxy. We have used our suite of SED models to estimate the color transformation from their ground-based $J − K_s$ to our NICMOS $J_{110} − H_{160}$ color. Roughly, the Kodama et al. bright red galaxies fall where the RDCS 1252 passive line crosses our color cut at $J_{110} − H_{160} = 1.1$. This result hints at a possible bimodality in the red galaxy population of this protocluster, namely, that there are faint red galaxies that are inconsistent with passively evolving cluster members either due to large amounts of dust or due to higher redshifts of formation but that the more luminous protocluster members may have already finished forming and seem consistent with passive evolution to the present day.

7. DISCUSSION

We have identified a (6.2 times) surface overdensity and a corresponding photometric redshift "spike" of red $J_{110} − H_{160}$ galaxies that are likely associated with a known protocluster at $z = 2.16$. The optical-NIR spectral energy distributions of these sources suggest that they comprise both evolved galaxies as well as dust-obscured star-forming galaxies. Based on our SED fits from the photometric redshift determinations, the approximate luminosity-weighted ages of these sources lie between 1 and 2.5 Gyr, and their stellar masses are of the order of a few times 10^{10} $M_{\odot}$. Detailed modeling of the SEDs for the protocluster population, along with their morphologies, is reserved for a future paper.

Comparison with the CMRs of lower redshift clusters shows that the red galaxy overdensity primarily lies blueward of the no-evolution predictions. That the red galaxies in 1138 are also redder than the $z_{form} \sim 3$ case suggests both that there are galaxies with significant dust content, an assertion supported by the SED fits, and also that they were perhaps formed at higher redshift than the RDCS 1252 galaxies. Of course, without a classical, low-scatter red sequence to use as a baseline there remains considerable uncertainty in the age of the population as a whole. The results of Steidel et al. (2005) suggest that protocluster galaxies are older than their "field" counterparts at $z \sim 2.3$ and that these ages and stellar masses were broadly consistent with evolution to

lower redshift cluster galaxies. However, their protocluster members were all UV selected and star forming. With future spectroscopy of our red galaxy sample it will be possible to see if these differences persist when looking at a more varied galaxy sample.

For three samples of galaxies drawn from the full H_{160}-band–selected data set we have fit a color-magnitude relation and estimated the intrinsic scatter. The CMR at $z = 2.16$ is not as well defined as at $z \sim 1$ or 0. For sample C, made up of seven galaxies, the color, best-fit spectral template, morphology, and photo-z all point toward them being (proto)elliptical galaxies within the protocluster. For this small sample, the estimated intrinsic scatter is rather low and may suggest that these galaxies represent the forming red sequence in this protocluster. The slope of this relation is extremely steep compared to lower redshift clusters. The slope of the CMR is generally assumed to be a manifestation of the mass-metallicity relation and would therefore flatten at higher redshift. The major caveat regarding the steep slope of sample C is that none of these galaxies are spectroscopically confirmed protocluster members. Therefore, this "relation" may just be a random, although somewhat unlikely, coincidence rather than a nascent CMR. However, further deep NIR imaging coverage of this field is required to identify additional members of this protoelliptical galaxy class.

REFERENCES

Bell, E. F., et al. 2004, ApJ, 608, 752
Benítez, N. 2000, ApJ, 536, 571
Bertin, E., & Arnouts, S. 1996, A&AS, 117, 393
Blakeslee, J. P., et al. 2003, ApJ, 596, L143
———. 2006, ApJ, 644, 30
Bruzual, G., & Charlot, S. 2003, MNRAS, 344, 1000
Croft, S., Kurk, J., van Breugel, W., Stanford, S. A., de Vries, W., Pentericci, L., & Röttgering, H. 2005, AJ, 130, 867
de Jong, R. 2006, Correcting the NICMOS Count-Rate Dependent Nonlinearity (Instrum. Sci. Rep. 2006-003; Baltimore: STScI)
Dickinson, M., et al. 2000, ApJ, 531, 624
Faber, S. M., et al. 2007, ApJ, 665, 265
Gladders, M. D., & Yee, H. K. C. 2005, ApJS, 157, 1
Gobat et al. 2008, A&A, submitted
Grazian, A., et al. 2007, A&A, 465, 393
Kodama, T., Tanaka, I., Kajisawa, M., Kurk, J., Venemans, B., De Breuck, C., Vernet, J., & Lidman, C. 2007, MNRAS, 377, 1717
Krist, J. 1993, in ASP Conf. Ser. 52, Astronomical Data Analysis Software and Systems II, ed. R. J. Hanisch, R. J. V. Brissenden, & J. Barnes (San Francisco: ASP), 536
Kurk, J. D. 2003, Ph. D. thesis, Leiden Univ.
Kurk, J. D., Pentericci, L., Overzier, R. A., Röttgering, H. J. A., & Miley, G. K. 2004a, A&A, 428, 817

Kurk, J. D., Pentericci, L., Röttgering, H. J. A., & Miley, G. K. 2004b, A&A, 428, 793
Miley, G. K., et al. 2006, ApJ, 650, L29
Mullis, C. R., Rosati, P., Lamer, G., Böhringer, H., Schwope, A., Schuecker, P., & Fassbender, R. 2005, ApJ, 623, L85
Oke, J. B. 1974, ApJS, 27, 21
Peng, C. Y., Ho, L. C., Impey, C. D., & Rix, H.-W. 2002, AJ, 124, 266
Pentericci, L., Kurk, J. D., Carilli, C. L., Harris, D. E., Miley, G. K., & Röttgering, H. J. A. 2002, A&A, 396, 109
Sérsic, J. L. 1968, Atlas de Galaxias Australes (Cordoba: Obs. Astron.)
Stanford, S. A., et al. 2005, ApJ, 634, L129
———. 2006, ApJ, 646, L13
Steidel, C. C., Adelberger, K. L., Shapley, A. E., Erb, D. K., Reddy, N. A., & Pettini, M. 2005, ApJ, 626, 44
Stevens, J. A., et al. 2003, Nature, 425, 264
Thompson, R. I., et al. 2005, AJ, 130, 1
Tremonti, C. A., et al. 2004, ApJ, 613, 898
van Dokkum, P. G., & van der Marel, R. P. 2007, ApJ, 655, 30
Venemans, B. P., et al. 2007, A&A, 461, 823
Zirm, A. W., et al. 2007, ApJ, 656, 66